2019-11-01

Hydrodynamic X-Waves

James N. Steer[1], Alistair G. L. Borthwick[1], Miguel Onorato[2], Amin Chabchoub[3], Ton S. van den Bremer[4]
1. School of Engineering, University of Edinburgh, Edinburgh EH9 3FB, UK.
2. Dipartimento di Fisica, Università di Torino and INFN, Sezione di Torino, Via Pietro Giuria 1, 10125 Torino, Italy.
3. Centre for Wind, Waves and Water, School of Civil Engineering, The University of Sydney, Sydney, NSW 2006, Australia.
4. Department of Engineering Science, University of Oxford, Oxford OX1 3PJ, UK
(Dated: August 10, 2019)

Stationary wave groups exist in a range of nonlinear dispersive media, including optics, Bose-Einstein condensates, plasma, and hydrodynamics. We report experimental observations of nonlinear surface gravity X-waves, i.e., X-shaped wave envelopes that propagate over long distances with constant form. These can be described by the 2D+1 nonlinear Schrödinger equation, which predicts a balance between dispersion and diffraction when the envelope (the arms of the X) travel at $\pm\arctan(1/\sqrt{2}) \approx \pm 35.26^\circ$ to the carrier wave. Our findings may help improve understanding the lifetime of extremes in directional seas and motivate further studies in other nonlinear dispersive media.

Stationary or nondispersive wave groups can occur in a range of nonlinear dispersive media, including in optics [1–3], Bose-Einstein condensates [4], plasma [5] and hydrodynamics. In optics, the free-space scalar wave equation has traditionally been used to investigate linear, localized waves (LWs), and a number of families of linear LW solutions have been found [6–8]. One such family is the so-called "X-wave" characterized by an X-shaped packet structure with a sharp, high amplitude centroid. Linear X-waves have been observed and confirmed to be nondispersive in optical fibres [9]. Optical LWs play a role in free space communications [10], optical lithography [11], and optical rogue waves [12].

When the scales of group velocity dispersion (GVD) and nonlinear amplitude effects are comparable, nonlinearity must be considered. Whereas GVD can be described using a dispersion relationship, amplitude-dependent nonlinear effects are typically modelled through the universal nonlinear Schrödinger equation (NLSE) [13], which applies in nonlinear dispersive media [14, 15], and can be extended to two spatial dimensions to allow multi-dimensional, nonlinear LW group solutions. Indeed, in optics, "light bullet" nonlinear X-waves have been predicted and created experimentally [1, 2], and extreme LW events or 'rogue waves' have been detected in optical telecommunication fibres [16]. Due to the dispersive and nonlinear character of water waves, an analogy between water waves, optics, Bose-Einstein condensates and plasma can be naturally drawn [3, 17–20].

Both the coupled NLSE (CNLSE) (whereby two nonlinear wave systems interact) and the 2D+1 NLSE (whereby one wave system exists with a crossing angle θ between the carrier and envelope) can describe the evolution of crossing, weakly nonlinear wave systems. Using the 2D+1 NLSE, a critical crossing angle of $\theta_c = \pm \arctan 1/\sqrt{2}$ can be derived, beyond which linear focusing becomes defocusing, and the system achieves stability to sideband perturbations [21]. In the CNLSE, a similar stabilization of the coupled system is observed at the same critical angle [22]. For hydrodynamics and at low interaction angles, numerical simulations of the potential-flow Euler equations and experimentation have confirmed these predictions, observing an increase in the kurtosis of crossing seas up to approximately $\pm 25^\circ$ that reduces rapidly as the angle increased towards θ_c [23]. These results have been confirmed using phase-resolving numerical simulations for realistic broadbanded crossing sea states, showing that the maximum value of the kurtosis is small at the critical angle, with the minimum occurring at slightly larger angles [24].

In hydrodynamics, wave groups propagating at the critical crossing angle predicted by the 2D+1 NLSE occur naturally at the fringes of the Kelvin ship wake [25]. Furthermore, an isolated spectral energy peak tends to spread outwards at this angle [26]. Extreme wave heights in crossing seas are enhanced by second-order bound waves causing wave-averaged set-up [27]. Through the elimination of dispersion at the critical angle, it may be possible to extend dramatically the lifetime of groups containing extreme events. Indeed, previous numerical studies on the three-dimensional evolution of long-crested waves perturbed using random phases have shown natural formation of slanted coherent structures [28] that interact to produce long-lived rogue waves [29, 30].

In this experimental study, we create for the first time a nondispersive hydrodynamic X-wave; we do so in a directional and circular water-wave facility using the critical crossing angle. We measure the spatio-temporal free surface elevation of the X-wave, compare it with a numerical solution of the 2D+1 NLSE, and alter the crossing angle in order to quantify its effect on dispersion.

Theoretical background - We consider the two-dimensional nonlinear Schrödinger equation (2D+1

NLSE) for deep-water surface gravity waves [31]:

$$i\left(\frac{\partial A}{\partial t}+c_g\frac{\partial A}{\partial x}\right)-\alpha\frac{\partial^2 A}{\partial x^2}+2\alpha\frac{\partial^2 A}{\partial y^2}-\beta|A|^2A=0, \quad (1)$$

where x and y are the horizontal coordinates, t is time, and $A(x,y,t)$ the envelope of a carrier wave of frequency ω_0 and wavenumber $\boldsymbol{k}_0=(k_0,0)$ propagating in the x-direction. The coefficients of the 2D-NLSE are given by,

$$c_g=\frac{\partial\omega}{\partial k_x}\Big|_{\boldsymbol{k}=\boldsymbol{k}_0}=\frac{\omega_0}{2k_0},\ \alpha=\frac{1}{2}\frac{\partial^2\omega}{\partial k_x^2}\Big|_{\boldsymbol{k}=\boldsymbol{k}_0}=\frac{\omega_0}{8k_0^2},\ \beta=\frac{\omega_0 k_0^2}{2}. \quad (2a,b,c)$$

While the second derivative in the x-coordinate is responsible for the dispersion of the envelope, the second derivative in the y-coordinate implies diffraction. The leading-order identity $\partial A/\partial t\simeq -c_g\partial A/\partial x$ can be used to transform the 2D+1 NLSE to a form that is a more suitable framework for laboratory experiments [32, 33],

$$i\left(\frac{\partial A}{\partial x}+\frac{1}{c_g}\frac{\partial A}{\partial t}\right)-\frac{\alpha}{c_g^3}\frac{\partial^2 A}{\partial t^2}+\frac{2\alpha}{c_g}\frac{\partial^2 A}{\partial y^2}-\frac{\beta}{c_g}|A|^2A=0. \quad (3)$$

We look for solutions that correspond to envelopes traveling at an angle θ with respect to the carrier wave, which can be introduced through the transformation $T\equiv t\cos\theta+y\sin\theta/c_g$, giving from (3),

$$i\left(\frac{\partial A}{\partial x}+\frac{\cos\theta}{c_g}\frac{\partial A}{\partial T}\right)-\frac{\alpha}{c_g^3}(1-3\sin^2\theta)\frac{\partial^2 A}{\partial T^2}-\frac{\beta}{c_g}|A|^2A=0, \quad (4)$$

i.e., the integrable 1D+1 NLSE with a new coefficient in front of the dispersive term, $\alpha'\equiv\alpha(1-3\sin^2\theta)/c_g^3$. It can be seen that at $\theta=\pm\theta_c=\pm\arctan(1/\sqrt{2})\approx\pm35.26°$, the dispersive term becomes zero, then switches sign becoming defocusing [26, 34]. This is the critical crossing angle examined experimentally in this paper.

For small-amplitude waves, the nonlinear term in (4) can be neglected, and we have a dispersive linear Schrödinger equation. If $\theta=\pm\theta_c$, the system also becomes nondispersive ($\alpha'=0$), and the solution can be written as the superposition of two solutions, $A^+=A(x,T;\theta_c^+)$ and $A^-=A(x,T;\theta_c^-)$ with $\theta_c^+=+\theta_c$ and $\theta_c^-=-\theta_c$,

$$A(x,y,t)=A_0e^{-\left(t\cos\theta_c^+ +\frac{y}{c_g}\sin\theta_c^+-\frac{x\cos\theta_c^+}{c_g}\right)^2/(2\sigma^2)}+A_0e^{-\left(t\cos\theta_c^- +\frac{y}{c_g}\sin\theta_c^--\frac{x\cos\theta_c^-}{c_g}\right)^2/(2\sigma^2)}, \quad (5)$$

where A_0 is the theoretical linear focused amplitude of each arm, $\sigma^*\equiv\sigma/\cos(\theta_c)$ is the width of the group in the time domain, and we have chosen Gaussian envelopes. Equation (5) forms the characteristic linear nondispersive X-shape pattern illustrated in fig. 1. In the wavenumber spectrum of (5), all non-zero components are confined to the lines $k_y=\pm(k_x-k_0)\tan\theta_c$. The

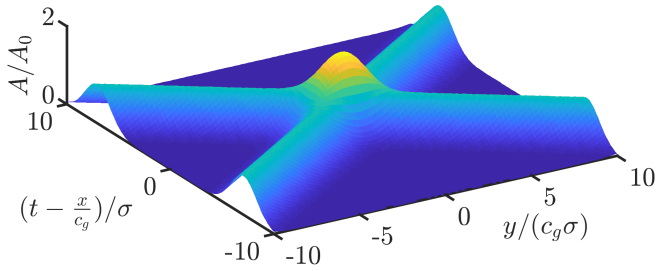

FIG. 1. Theoretical X-wave envelope solution formed by two Gaussian envelopes, as parameterized in (5).

critical angle also corresponds to the stability boundary of a uniform wave train [34, 35]. Single crossed-wave groups travelling at the critical angle can therefore be expected to travel without changing shape, as they are both unaffected by GVD and spectral sideband instabilities (see Supplementary Material, hereafter S.M.). Due to energy transfer from their highly centralized energy peak, double-crossed wave groups may experience non-stationary behaviour, as there are enough components to take part in four-wave interactions [26, 36]. *Experimental methodology* - In order to examine the effects of crossing at large angles, we carried out experiments in the circular FloWave Ocean Energy Research Facility at the University of Edinburgh (see S.M., fig. S3). This multi-directional wave basin has a 25 m diameter, is 2 m deep and is encircled by 168 actively absorbing wavemakers, enabling creation of waves in all directions. We adopt a Cartesian coordinate system with origin at the centre of the tank. In all experiments, the x-axis is in the direction of the phase velocity of the carrier waves. Wave gauges were spaced evenly along the x-axis, mounted to a gantry capable of moving in the y-axis (see S.M. fig. S3). Experiments were sufficiently short that reflections did not interfere with incident measurements.

To define a single crossed-wave group, we chose a narrow-banded Gaussian amplitude spectrum in frequency space,

$$\hat{A}(\omega)=\frac{A_0\sigma^*}{\sqrt{2\pi}}\exp\left(-\frac{(\omega-\omega_0)^2{\sigma^*}^2}{2}\right), \quad (6)$$

where σ^* is now more generally the length of the group in the time domain, and (6) corresponds to the Fourier transform of a single arm in (5) at $x=y=0$. The spectral bandwidth ($1/\sigma^*$) was set as large as possible to encourage dispersion at non-critical angles while keeping the group narrow-banded and avoiding distortion of the signal due to the minimum frequency cut-off $\omega_{\min}$ (corresponding to $k_{\min}$; see S.M.).

Table I summarizes all the experiments conducted, distinguishing two main types: single crossed-wave groups (expts. 1a-d and 2a-d), consisting of only a positive arm, and X-wave groups, consisting of both arms (expt.

3). Both lower-steepness (expts. 1a-d) and higher-steepness (expts. 2a-d) single crossed-groups were tested, while X-wave group experiments were always of a higher-steepness. A (non-dimensional) spatial nonlinear scale, $\lambda_{\mathcal{N}} = c_g/(\lambda_0\beta|A_0|^2)$ (derived from the nonlinear time scale) allows the number of wavelengths over which nonlinear effects take place to be estimated for each experiment. For the single crossed-group experiments, the crossing angle θ was varied while keeping the length of the group in time σ^* constant. Each experiment was repeated four times. See S.M. for further details.

Expt.	θ (°)	ω_0 (rad s^{-1})	$k_0 d$	σ^* (s)	$\epsilon_{\min}$	$\epsilon_{\max}$	$\lambda_{\mathcal{N}}$
1a	0				0.08	0.09	24.9
1b	$\theta_c^+/2$				0.08	0.09	24.9
1c	θ_c^+	7.07	10.2	2.29	0.08	0.09	24.9
1d	40				0.08	0.08	24.9
2a	0				0.17	0.25	5.6
2b	$\theta_c^+/2$				0.17	0.24	5.6
2c	θ_c^+	7.07	10.2	2.29	0.17	0.19	5.6
2d	40				0.17	0.16	5.6
3	θ_c^+ and θ_c^-	7.07	10.2	2.29	0.18	0.26	5.0

TABLE I. Experimental parameters, with $\epsilon_{\min}$ and $\epsilon_{\max}$ denoting the minimum and the maximum estimated steepness values ($\epsilon \equiv k_0|A|_{\max}$) and $\lambda_{\mathcal{N}}$ the estimated non-dimensional nonlinear spatial scale.

Results - For both single crossed-wave groups and X-waves, we compare our experimental results with numerical solutions of the 2D+1 NLSE (split-step Fourier method), using as the boundary condition the complex wavepacket amplitude at the first gauge (smallest x). We obtain this from the recorded free surface using $A = (\eta + i\tilde{\eta})\exp(-i(k_0 x - \omega_0 t))$, where $\tilde{\eta}$ is the Hilbert-transform of the free surface elevation η (e.g. [32]). For single crossed-wave groups, fig. 2 presents time series of the experimental and numerical packet envelope (see fig. S5, S.M. for spectra). In many cases, the indicative confidence bands obtained from 4 repeats of each experiment are not clearly visible due to their proximity to the mean, indicating very good repeatability of experiments. We introduce two quantitative measures of dispersion: maximum group amplitude and group width, which we define through the focus time, $t_f \equiv \sum_{i=1}^{N} t_i A_i / \sum_{i=1}^{N} A_i$, in the form of a standard deviation, as,

$$t_\sigma \equiv \sqrt{\frac{\sum_{i=1}^{N} (t_i - t_f)^2 A_i}{\sum_{i=1}^{N} A_i}}, \tag{7}$$

where the indicator i corresponds to the discrete sampling points in time. Figure 3 shows the change in the maximum amplitude and the group width from (7) as a function of evolution distances for different crossing angles.

In the lower-steepness case, both experimental and numerical unidirectional packets show clear focusing (fig. 2a) across approximately $10\lambda_0$ of evolution, including a decrease in group width as the group undergoes dispersive focusing (fig. 3b). At half the critical angle, the packet shows behaviour very similar to unidirectional (figs. 2b,3b), as expected based on the linear dispersion relationship (see fig. S1b, S.M.). At the critical crossing angle, the wave group amplitude only increases minimally (fig. 2c), and the width stays constant across the evolution distance (fig. 3b). Beyond the critical angle, at 40°, changes in the packet amplitude are still within one standard deviation (fig. 2d), and the width stays constant with minimal changes also predicted by linear theory (see fig. S1b, S.M.). For all angles, behaviour is well predicted by the 2D+1 NLSE and predominantly linear, as can be confirmed by the absence of significant spectral changes across the evolution distance (see fig. S5a-d, S.M.).

In the higher-steepness cases, the unidirectional (fig. 2e) and $\theta = \theta_c^+/2$ (fig. 2f) experiments show much more substantial focusing than their lower-steepness counterparts. Nonlinear changes are very likely to have occurred, as is evident from the significant spectral changes (fig. S5e,f, S.M.), including a drop in peak spectral amplitude and significant spectral widening as a classical signature of modulational instability. The 2D+1 NLSE (black lines) with its restrictions on steepness and bandwidth captures the main features but not all aspects of the observed behaviour for these higher-steepness, close-to-unidirectional cases.

The time domain behaviour of the higher-steepness critical angle experiment (fig. 2g) appears to show some changes in the packet shape, with larger waves moving to the front of the group creating a double-peak, but the maximum amplitude of the packet remains largely unchanged (fig. 3c). The nullification of the dispersive term in the 2D+1 NLSE at the critical angle has removed linear focusing and stabilized the wave group, as predicted by linear stability analysis (cf. (S2) and fig. S2, S.M.). Beyond the critical angle, at 40° (fig. 2h), we observe very similar behaviour. The numerical solution of the 2D+1 NLSE shows these effects clearly with a completely stationary wave group in the group frame for the critical angle (fig. 2g).

Summarizing, it is clear from fig. 3c,d that, as with the lower-steepness experiments, the behaviour of the 35.26° and the 40° cases are least dispersive, as well predicted by the 2D+1 NLSE, and that most of the strong nonlinearity observed for small and zero angles is quelled for these larger crossing angles. For the higher-steepness experiments, spectral changes occur that are somewhat greater than predicted by the 2D+1 NLSE or small but non-zero where zero changes are predicted by the 2D+1 NLSE (fig. S5e-h, S.M.).

Turning from the single-crossed to the double-crossed or X-waves (expt. 3), we reconstruct surfaces of measured packet amplitude $A(y,t)$ at different gauge loca-

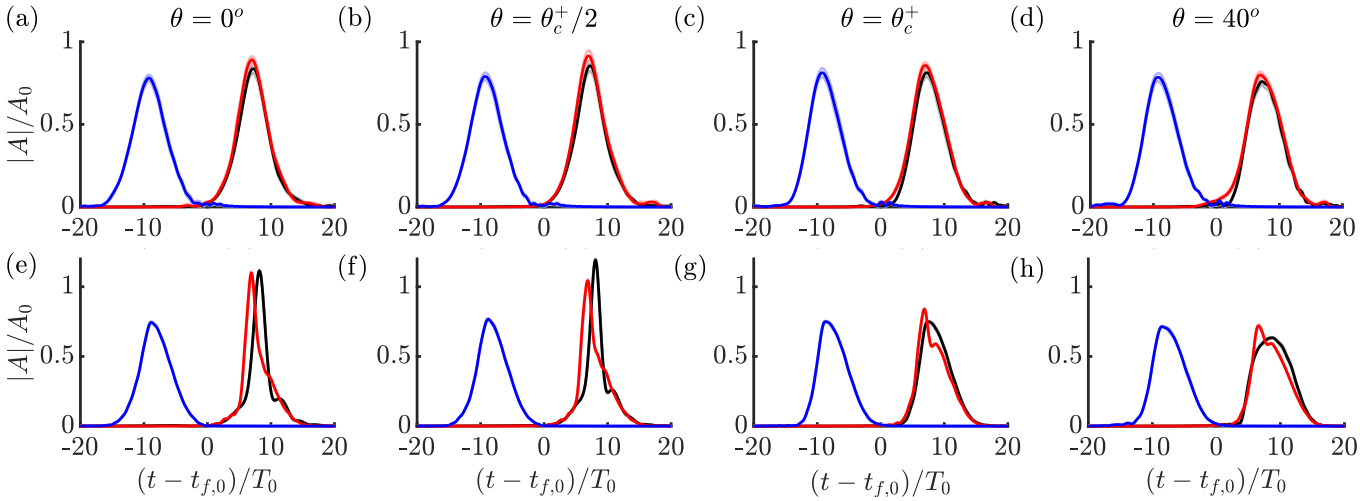

FIG. 2. Envelope time series (normalized by the carrier period, T_0) for the single crossed-wave lower-steepness experiments 1a-d (a-d) and the higher-steepness experiments 2a-d (e-h). Blue, red and black lines denote experiments at the initial ($x/\lambda_0 = -6.67$) gauge, and experiments and numerical solutions at the final ($x/\lambda_0 = 3.60$) gauge, respectively. The dark and light lines show the mean and the confidence bands (± one standard deviation). Confidence bands may be difficult to distinguish in some panels due to strong repeatability.

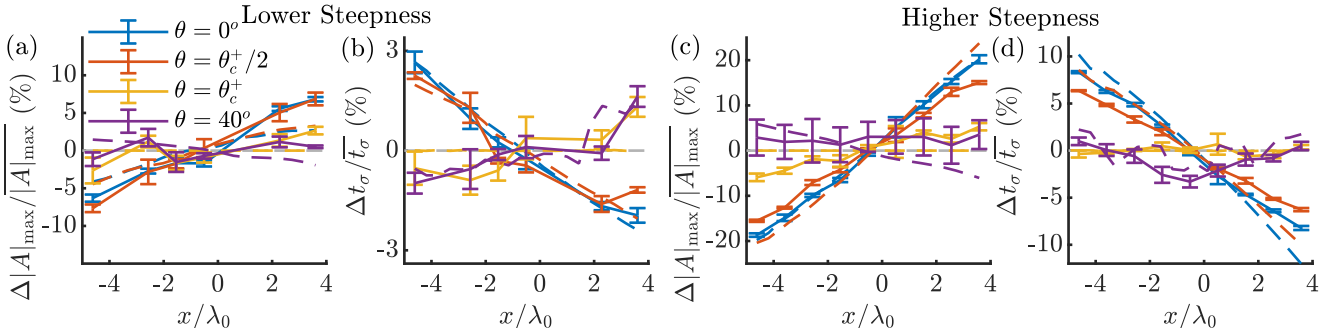

FIG. 3. Relative change of the maximum packet amplitude $\Delta|A|_{\max} = |A|_{\max} - \overline{|A|_{\max}}$ (a,c) and the group width $\Delta t_\sigma = t_\sigma - \overline{t_\sigma}$ (b,d) in space for different crossing angles, where $\overline{|A|_{\max}}$ and $\overline{t_\sigma}$ denote averages across the gauges, and t_σ is defined by (7). Panel a,b shows experiments 1a-d (lower-steepness), and panel c,d experiments 2a-d (higher-steepness). The continuous and dashed lines denote the mean across repeat experiments with error bars (± one standard deviation) and numerical solutions, respectively.

tions and compare with numerical solutions and corresponding spectra $\hat{A}(\omega, k_y)$, as shown in fig. 4. At the beginning of its evolution (top rows), the experimental X-wave structure is clearly visible with distinct arms lying on the $\pm\theta_c$ lines and a centroid of amplitude $2A_0$. The X-structure maintains its global shape as it propagates across the tank, although the finite number of straight wave paddles and potential reflections makes perfect generation by constructive super-positioning away from the centre and near the boundaries of the tank challenging (cf. large-time behaviour in fig. 4).

For this higher-steepness experiment, the peak at the crossing points of the two arms undergoes considerable narrowing in the x-direction (its direction of travel, shown here as time t) and broadening in the y-direction, a phenomenon previously observed by Gibbs & Taylor for directionally spread groups that are not crossing and described therein as 'walls of water' [37]. We observe this behaviour in both experiments and numerical simulations of the 2D+1 NLSE and note that it arises because of resonant third-order nonlinearity from the interaction between four wave components [36]. Accordingly, the 2D+1 NLSE predicts a preferential energy transfer to higher wavenumbers, as shown in the right column of fig. 4. Unlike the single crossed-wave groups, where all the non-zero spectral components are confined to a single line, the double-crossed or X-wave has sufficient components to take part in four-wave interaction (cf. Phillips's figure of 8), which for a narrow-banded three-dimensional wave packet has the largest preferential direction of energy transfer to higher-wavenumbers at 35.26° [26]. An extended set of numerical solutions for single crossed-

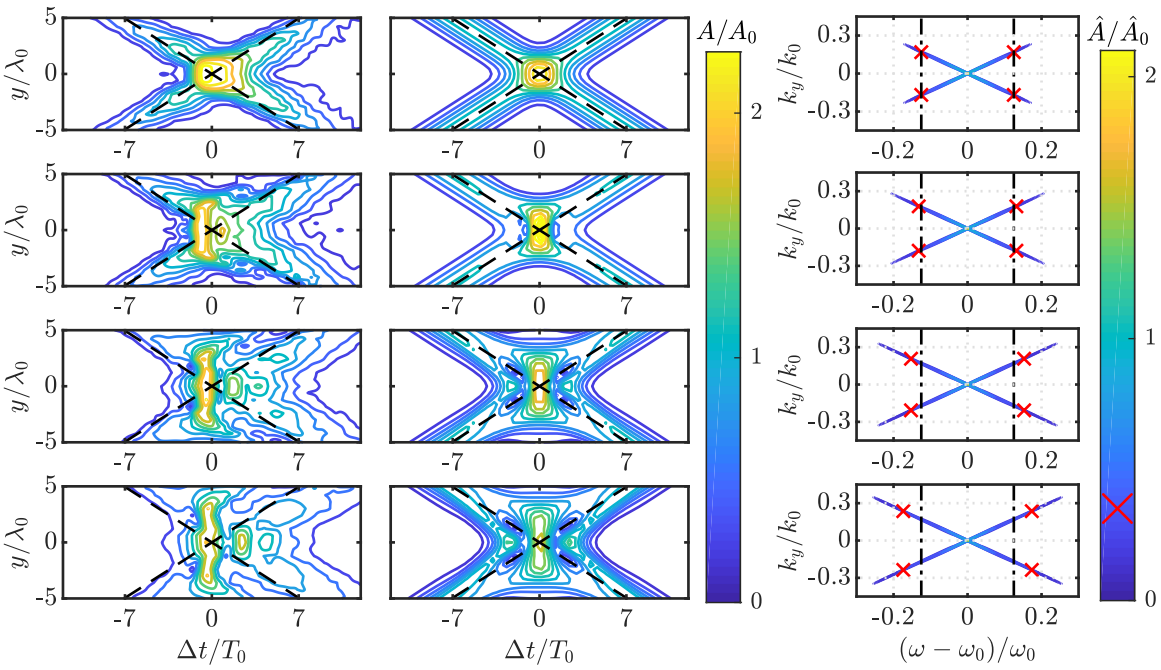

FIG. 4. Spatio-temporal comparison of the experimental (left) and numerical (centre) X-wave packet (expt. 3) as the packet evolves in space: $\Delta x/\lambda_0 = -9.6,\ -3.2,\ 1.9,\ 4.4$ (rows, descending). The black dashed lines corresponds to the 35.26° angle. The amplitude spectra $\hat{A}(\omega, k_y)$ of the numerical results are also presented (right): grey lines are grid lines, red crosses indicate the position of the contour at $\hat{A}/\hat{A}_0 = 0.33$ with the back dash-dotted lines aligned with the crosses in the top panel. We show the spatio-temporal signals in the group reference frame as predicted by linear theory.

groups and X-waves confirms that the 2D+1 NLSE predicts truly stationary behaviour for single-crossed waves at 35.26°; the most long-lived X-waves occur at angles close to 35.26° for small-steepness, with the angle of maximum lifetime increasing up to approximately 45° for higher steepness (see figs. S6 and S7, S.M.).

Conclusion - We have experimentally demonstrated the existence of nondispersive single crossed-wave groups and long-lived nonlinear hydrodynamic X-wave packets when a carrier wave is modulated by a wave group crossing it at an angle of approximately ±35.26°, as predicted by the 2D+1 NLSE and previously observed experimentally in optics. Our single crossed-wave group experiments showed no linear or nonlinear focusing at the critical angle, with both amplitude and group width remaining constant across the evolution distance regardless of steepness, as predicted by numerical solutions of the 2D+1 NLSE.

When the two arms travelling at ±35.26° are superimposed, a nondispersive hydrodynamic X-wave is constructed, which we have observed in the laboratory. Such a structure was observed to be quasi-stationary for a relatively high steepness, however became subject to third-order resonant four-wave interactions, which are known to transfer energy to higher wavenumbers with a preferred direction of ±35.26° [26] and result in the most long-lived X-wave structures at angles ±35.26° for small steepness, increasing up to approximately ±45° for higher steepness. In the real ocean, such bimodal seas, with energy travelling in two directions, do not occur infrequently [38], and this preferred growth direction may lead to the natural generation of X-waves, which in turn will be long-lived due to their lack of dispersion. Although unidirectional groups focused to more extreme amplitudes, the experimental observation of crossed groups propagating unchanged over many wavelengths confirm the lifetime extension of wave groups containing the potential for extreme events.

Finally, this work may motivate new numerical and experimental studies to investigate the applicability of directional coherent structures in different nonlinear dispersive physical media known to be described by the NLSE, where such structures have not yet been observed, such as plasma, Bose-Einstein condensates and cold gases.

Acknowledgements - The authors thank Mr E. Nixon, Dr S. Draycott, and Dr T. Davey at FloWave. FloWave was funded by the UK EPSRC (EP/I02932X/1). JNS acknowledges an EPSRC studentship (No. 1770088), and TSvdB a Royal Academy of Engineering Research Fellowship. AC acknowledges Takuji Waseda for valuable discussions. MO has been funded by Progetto di Ricerca d'Ateneo CSTO160004 and supported by the "Department of Excellence 2018-2022" Grant awarded by the

Italian Ministry of Education, University and Research (MIUR) (L.232/2016).

[1] C. Conti, S. Trillo, P. Di Trapani, G. Valiulis, A. Piskarskas, O. Jedrkiewicz, and J. Trull, Nonlinear electromagnetic x waves, Phys. Rev. Lett. **90**, 170406 (2003).

[2] P. Di Trapani, G. Valiulis, A. Piskarskas, O. Jedrkiewicz, J. Trull, C. Conti, and S. Trillo, Spontaneously generated x-shaped light bullets, Phys. Rev. Lett. **91**, 093904 (2003).

[3] F. Baronio, S. Wabnitz, and Y. Kodama, Optical Kerr spatiotemporal dark-lump dynamics of hydrodynamic origin, Phys. Rev. Lett. **116**, 173901 (2016).

[4] V. V. K. Yu. V. Bludov and N. Akhmediev, Matter rogue waves, Phys. Rev. A **80**, 033610 (2009).

[5] Y. N. H. Bailung, S.K. Sharma, Observation of Peregrine solitons in a multicomponent plasma with negative ions, Phys. Rev. Lett. **107**, 255005 (2011).

[6] J. N. Brittingham, Focus waves modes in homogeneous Maxwells equations: Transverse electric mode, J. Appl. Phys. **54**, 1179 (1983).

[7] R. W. Ziolkowski, Exact solutions of the wave equation with complex source locations, J. Math. Phys. **26**, 861 (1985).

[8] R. W. Ziolkowski, Localized transmission of electromagnetic energy, Phys. Rev. A **39**, 2005 (1989).

[9] J. Lu and J. F. Greenleaf, Nondiffracting X waves-exact solutions to free-space scalar wave equation and their finite aperture realizations, IEEE T. Ultrason. Ferr. **39**, 19 (1992).

[10] H. A. Willebrand and B. S. Ghuman, Fiber optics without fiber, IEEE Spectrum **38**, 40 (2001).

[11] T. Ito and S. Okazaki, Pushing the limits of lithography, Nature **406**, 1027 (2000).

[12] D. Solli, C. Ropers, P. Koonath, and B. Jalali, Optical rogue waves, Nature **450**, 1054 (2007).

[13] M. J. Ablowitz, *Nonlinear dispersive waves: asymptotic analysis and solitons*, Vol. 47 (Cambridge University Press, 2011).

[14] M. Onorato, S. Residori, U. Bortolozzo, A. Montina, and F. Arecchi, Rogue waves and their generating mechanisms in different physical contexts, Phys. Rep. **528**, 47 (2013).

[15] J. M. Dudley, F. Dias, M. Erkintalo, and G. Genty, Instabilities, breathers and rogue waves in optics, Nat. Photonics **8**, 755 (2014).

[16] F. Baronio, B. Frisquet, S. Chen, G. Millot, S. Wabnitz, and B. Kibler, Observation of a group of dark rogue waves in a telecommunication optical fiber, Phys. Rev. A **97**, 013852 (2018).

[17] A. Chabchoub, B. Kibler, C. Finot, G. Millot, M. Onorato, J. Dudley, and A. Babanin, The nonlinear Schrödinger equation and the propagation of weakly nonlinear waves in optical fibers and on the water surface, Ann. Phys. **361** (2015).

[18] M. Onorato, F. Baronio, M. Conforti, A. Chabchoub, P. Suret, and S. Randoux, Hydrodynamic and optical waves: A common approach for unidimensional propagation, in *Rogue and Shock Waves in Nonlinear Dispersive Media* (Springer, 2016) pp. 1–22.

[19] B. Kibler, A. Chabchoub, A. Gelash, N. Akhmediev, and V. E. Zakharov, Superregular breathers in optics and hydrodynamics: Omnipresent modulation instability beyond simple periodicity, Phys. Rev. X **5**, 41026 (2015).

[20] R. El Koussaifi, A. Tikan, A. Toffoli, S. Randoux, P. Suret, and M. Onorato, Spontaneous emergence of rogue waves in partially coherent waves: a quantitative experimental comparison between hydrodynamics and optics, Phys. Rev. E **97**, 012208 (2018).

[21] W. H. Hui and J. Hamilton, Exact solutions of a three-dimensional nonlinear Schrödinger equation applied to gravity waves, J. Fluid Mech. **93**, 117 (1979).

[22] M. Onorato, A. R. Osborne, and M. Serio, Modulational instability in crossing sea states: A possible mechanism for the formation of freak waves, Phys. Rev. Lett. **96**, 014503 (2006).

[23] A. Toffoli, E. M. Bitner-Gregersen, A. R. Osborne, M. Serio, J. Monbaliu, and M. Onorato, Extreme waves in random crossing seas: Laboratory experiments and numerical simulations, Geophys. Res. Lett. **38** (2011).

[24] E. B.-G. K. T. Gramstad, O. and J. N. Borge, Modulational instability and rogue waves in crossing sea states, J. Phys. Oceanogr. **48**, 1317 (2018).

[25] D. H. Peregrine, Water waves, nonlinear Schrödinger equations and their solutions, ANZIAM J. **25**, 16 (1983).

[26] M. S. Longuet-Higgins, On the nonlinear transfer of energy in the peak of a gravity-wave spectrum: a simplified model, Proc. R. Soc. Lond. A **347**, 311 (1976).

[27] M. L. McAllister, T. A. A. Adcock, P. H. Taylor, and T. S. van den Bremer, The set-down and set-up of directionally spread and crossing surface gravity wave groups, J. Fluid Mech. **835**, 131 (2018).

[28] V. P. Ruban, Enhanced rise of rogue waves in slant wave groups, JETP Lett+ **94**, 177 (2011).

[29] V. P. Ruban, Breathing rogue wave observed in numerical experiment, Phys. Rev. E **74**, 036305 (2006).

[30] V. Ruban, Nonlinear stage of the benjamin-feir instability: three-dimensional coherent structures and rogue waves, Phys. Rev. Lett. **99**, 044502 (2007).

[31] V. E. Zakharov, Stability of periodic waves of finite amplitude on the surface of a deep fluid, J. Appl. Mech. Tech. Phy. **9**, 190 (1968).

[32] A. Osborne, *Nonlinear Ocean Waves and the Inverse Scattering Transform* (Academic Press, 2010).

[33] A. Chabchoub and R. Grimshaw, The hydrodynamic nonlinear Schrödinger equation: Space and time, Fluids **1**, 23 (2016).

[34] P. G. Saffman and H. C. Yuen, Stability of a plane soliton to infinitesimal two-dimensional perturbations, Phys. Fluid. **21**, 1450 (1978).

[35] H. C. Yuen and B. M. Lake, Nonlinear dynamics of deep-water gravity waves (Elsevier, 1982) pp. 67–229.

[36] O. Phillips, On the dynamics of unsteady gravity waves of finite amplitude part 1. the elementary interactions, J. Fluid Mech. **9**, 193 (1960).

[37] R. Gibbs and P. Taylor, Formation of walls of water in 'fully' nonlinear simulations, Appl. Ocean Res. **27**, 142 (2005).

[38] K. Ewans, Observations of the directional spectrum of fetch-limited waves., J. Phys. Oceanogr. **28**, 495–512 (1998).